IEEE Access
Multidisciplinary ⋮ Rapid Review ⋮ Open Access Journal

Received February 2, 2022, accepted February 13, 2022, date of publication February 18, 2022, date of current version March 2, 2022.

Digital Object Identifier 10.1109/ACCESS.2022.3152777

On the Induced Currents to Wind Turbines by the Earth's Atmospheric Electric Potential: Experiments With Drones

POL FONTANES[1,2], **JOAN MONTANYÀ**[1], **MARCELO ARCANJO**[1,2], **MICHELE URBANI**[1], **CRISTIAN ASENSIO**[1], **AND CARMEN GUERRA-GARCIA**[3]

[1]Electrical Engineering Department, Universitat Politècnica de Catalunya, 08034 Barcelona, Spain
[2]Dena Desarrollos S.L. (Ingesco), 08223 Terrassa, Spain
[3]Aeronautics and Astronautics Department, Massachusetts Institute of Technology, Cambridge, MA 02139, USA

Corresponding author: Pol Fontanes (pol.fontanes@upc.edu)

This work was supported in part by the Research Grant from the Spanish Ministry of Economy EXPLORA Call under Grant ENE2017-91636-EXP, in part by the Massachusetts Institute of Technology (MIT) MISTI Global Seed Funds MIT-Spain Project "Smart Lightning Protection Systems for Wind Turbines and Aircraft" and "Small Unmanned Airborne Systems for Atmospheric Electricity Research," and in part by the Industrial Doctorate Grant of the AGAUR under Grant 2019 DI 039. The work of Marcelo Arcanjo and Michele Urbani was supported by the European Union's Horizon 2020 Research and Innovation Program under the Marie Sklodowska-Curie under Grant 722337.

ABSTRACT We live in an electrified atmosphere where a potential difference of about 250 kV is established between the ground and the ionosphere. The resulting potential gradient induces electric charges on the objects immersed in the atmosphere, which are more significant in tall objects. Several works have identified interferences to sensors in wind turbine rotor blades being attributed to electrostatic charging of blades. This paper presents a novel experiment using vertical wires lifted by a drone to study the currents resulting under fair-weather atmospheric conditions. Two current components are identified, one resulting in point/corona discharge and the other related to the movement. Based on the experimental results, a model for predicting induced currents on wind turbines is proposed, and estimates for thunderstorm conditions are made. The results presented in this paper are important for designing the electromagnetic compatibility measures to ensure the reliability of multi-megawatt wind turbines with blades equipped with active control systems and higher use of sensors.

INDEX TERMS Wind turbine, induced currents, drones, atmospheric current, point discharge, space charge, modeling, sensors.

I. INTRODUCTION

As the wind energy sector grows as a green and reliable energy source, considerable efforts are being made to improve performance while lowering costs [1]. To reduce maintenance costs, wind turbines are being fitted with a myriad of sensors that help monitor their status, referred to as condition monitoring systems (CMSs) [2]. Unfortunately, those sensors are vulnerable to the harsh environment that wind turbines have to withstand and are easily subject to faults. The three most common types of sensor faults are: *short faults*, or single-sample spikes in sensor readings; *constant faults*, also called *stuck-at faults*, associated with an anomalous constant offset at longer timescales and may indicate hardware malfunction; and *noise faults* when the noise level is unusually high [3].

Additionally, as wind turbines become larger the loading on the blades also increases [4]. Active flap systems (AFS) on multi-megawatt wind turbines have been validated to reduce the load impact on the blade and rotor and are expected to be installed in the following years [5]. These systems use the CMS sensors feedback to operate. Therefore, it is essential to minimize the sensor's faults in order to actuate the AFS properly.

A frequent external cause of failure for CMS sensors is damage from short-duration high current pulses from electrostatic discharges (ESD) [6]. Depending on the conditions and energy delivery by the ESD, the failure can be transient or fatal for the sensor. In the case of wind turbine blades, both under fair-weather and thunderstorm conditions, it is

The associate editor coordinating the review of this manuscript and approving it for publication was Fabio Mottola.

generally assumed that charging of the blade surface in the presence of wind is responsible for ESD that can pose hazards to sensors in the blade and cause interferences to other sensitive systems [7], [8]. However, ESD is triggered mainly by the electrification of the tall conductive structure when exposed to atmospheric electric fields and does not require wind presence. In addition to ESD hazards, this electrification can lead to induced currents on tall structures that can produce interferences in sensors, increasing the noise level or causing false readings [9].

Current solutions to mitigate sensor faults rely on the redundancy of sensors and fault detection algorithms as described in [3], [10], [11], and [12]. In these works, different methodologies based on statistical analysis are implemented to determine if the readings of the sensors are correct. On the one hand, this approach is powerful as it can remotely assess the correct or faulty operation of the sensors, and this is an advantage because sensors are typically placed in locations that are difficult and costly to access. However, this methodology does not provide much information on the cause of failure and cannot effectively predict future failures.

To understand how wind turbine sensors are affected by induced currents, it is necessary to understand their operational environment under different weather conditions. During thunderstorms, the electromagnetic environment can lead to significant sensor-disturbances due to lightning strikes or simply from the high quasi-electrostatic fields in the presence of thunderclouds [13], [14]. However, since wind turbines are very tall conductive towers, intense electric fields can develop at the tips of the blades even under fair-weather conditions [9]. That is because, under fair-weather, the Earth's atmospheric potential rapidly increases up to a few tens of kilovolts below 200 m altitudes, as measured by Hy-wire balloon experiments [15]. This potential drop induces charge to grounded tall objects by electrostatic induction, where the maximum induced charge is found at the tip of the grounded object. State-of-the-art wind turbines of more than 10 MW can reach altitudes of more than 200 m. This can result in electric field amplification at sharp edges [9], leading to point/corona discharge [16]. In addition, there is a periodic variation in the induced electrical charge due to the movement of the rotor, which induces currents, as explained in [9]. This same work presents an experimental study using kites tethered by conductive wires to simulate fair-weather induced charges and currents on the tall wind turbine. Experiments are backed up by numerical simulations, concluding that induced currents to 1.5MW and 5MW wind turbines can be in the range of nA to μA. However, this study ignored the possible occurrence of point/corona discharge and the deposition of charge on the massive dielectric components of wind turbines, which can lead to ESD-related risks to sensors and personnel. These effects can be significant, as revealed by experiments deploying cables with barrage balloons that measured electric currents originated by point/corona discharge on the cable ranging from microamperes to kiloamperes in fair and thunderstorm weather, respectively [17].

To motivate how induced currents on vertical wires can be used to model the wind turbine electrification process, the different building elements of the wind turbine and their relations will be reviewed in what follows. Wind turbines can be considered electrically conductive from the tip of the blade to the grounding system. Although blades are made of non-conductive glass fiber, the standard addition of carbon-reinforced components (e.g., spars) [18] as well as the required Lightning Protection System (LPS) [19] ensures the existence of a conductive path from the tip to the root. For that reason, prior works used tethered kites [9], and tethered balloons [17], to simulate the electrical behavior of wind turbines. However, a significant shortcoming with both platforms is the difficulty of maintaining a fixed position and keeping the tether oriented in the vertical direction.

Nowadays, multirotor drones allow vertical flight and hover (fixed-position) flight. The first experiments deploying vertical wires by multirotor drones were reported in [20], where we experimentally demonstrated that ESD on wind turbines could be energetic enough to damage electrical systems in wind turbine blades and nacelles. Those experiments revealed the potential, and relative simplicity, of the method to further study the electrification of wind turbines under different weather conditions. For that reason, we conducted a series of preliminary experiments where we deployed vertical conductors with drones to simulate wind turbines [21]. The first set of experiments showed that using a drone allowed for much better control of the wire position, geometry, altitude, and vertical speed, compared to kites or balloons, for which it is nearly impossible to ensure that the wire stays still and vertical. This allowed to qualitatively study induced currents in tall, grounded structures and charging on floating conductors. Results showed that two contributing factors to current induction in wind turbines are the variable vertical position of the blade tips moving at constant vertical speed as well as the appearance of point discharge. Motivated by those qualitative observations, this article presents quantitative experiments to study wind turbine-induced currents for grounded blades and makes use of the experimental data to elucidate the relative role of the blade tips' vertical speed and point/corona discharge. Extension to wind turbines with electrically isolated blades is left for future experiments. In addition, a model is derived for predicting wind turbine-induced currents under fair-weather conditions. It allows forecasting expected CMS sensor noise levels and possible failures because of ESD and high currents.

The paper is structured as follows. First, the experimental setup and methodology are described. Second, results from the experiments deploying vertical conductors are presented and analyzed, revealing the relationships between altitude, vertical speed, and induced current. Then the experimental results are compared to simple theoretical models to derive a model for predicting induced currents. Following, the results and analysis are discussed in terms of implications for wind turbines, and the model is extended for wind turbines and thunderstorm weather conditions. Furthermore, potential hazards to people and CMS sensors are discussed. The paper ends with the conclusions.

II. EXPERIMENTAL SETUP

From the base to the tips of the rotor blades, a wind turbine can be modeled as an electrically conductive thin wire [9]. This approximation applies even when some conductive parts are covered with insulation components, such as the down conductors hosted inside the insulating blades, as the LPS ensures the existence of a conductive path to the ground [18], [19].

In this paper, we propose a novel experimental method that uses a thin conductive wire to represent the electrical behavior of a wind turbine structure and down conductor under fair-weather conditions. The experiment is designed to measure induced currents on the wire while deploying it into the atmosphere to experimentally simulate the electrification mechanisms that affect a wind turbine with grounded blades.

The wire needs to maintain a vertical orientation to better represent the wind turbine geometry under dynamic and static conditions. The wire's static and deploying conditions need to be considered since wind turbines are affected by atmospheric electricity both while moving (blades rotating) or stopped [22]. The wire position and vertical speed are accurately controlled using a multirotor drone that deploys the wire upwards. Dynamically controlling the wire altitude allows recreating the variable height of the tip of a rotating wind turbine blade. Also, deploying different lengths of the wire can represent different wind turbine heights.

The experimental setup consists of a conductive wire stored in a spool with a shaft that allows the wire to be unspooled when the drone exerts tension to it. The spool is electrically isolated from the ground using a PTFE support, and one end of the wire is grounded through a pico-ammeter (RBD 9103) while the other is attached to the drone (Figure 2 and Figure 3). Electrically isolating the spool of wire ensures that the measured induced currents can only come from the grounded end, which is monitored, and not from other unknown contact sources. The wire attached to the drone is tied using 10m of electrically isolating Kevlar wire. The 10m of Kevlar wire was selected to avoid the drone's rotors wind influence. This length was determined experimentally by measuring the vertical air velocity with an anemometer at the ground under the drone for different flight altitudes. The measurements confirmed that the drone's airstream could not be detected for separation beyond 5m between the drone and the tip of the wire.

The conductive wire used to measure the induced currents is an RG174 coaxial cable where the outer insulation jacket and the ground braid have been removed, leaving the inner copper conductor and its dielectric insulator. The objective of keeping the insulator is to ensure that, in the event of point/corona discharge occurrence, this discharge would be located at the tip, such as was found in [15], and not along the conductor length. The measured resistance of the wire is $0.14\Omega/\mathrm{m}$, determined as the average resistance of 10 different sections of 1m of the wire, measured with a 34401A Digital Multimeter. The value measured is consistent with that provided by the manufacturer, $0.1426\Omega/\mathrm{m}$.

In an idealized manner, the geometry of the tip of the wire emulates the sharpness of the wind turbine blade tip, and the study of induced currents for different geometries can inform how it can influence the electrification process. For that reason, we use two different electrodes at the tip of the wire attached to the drone: a sharp needle and a rounded tip. The electrodes consist of a 3mm rounded steel rod and a 0.5mm steel needle (Figure 1). Note that the radius of curvature at the needle tip is significantly smaller than 0.25mm. This is important for the model simulation analysis performed later in the article since point/corona discharge is expected to occur at the tip. The use of different electrodes for the tip and selection of their sizes was informed by observations in [23], where sharp needles were found to start point/corona discharge at lower threshold voltages than rounded ones. For the flights reported in this paper, the electrode used in each flight is indicated in Table 1.

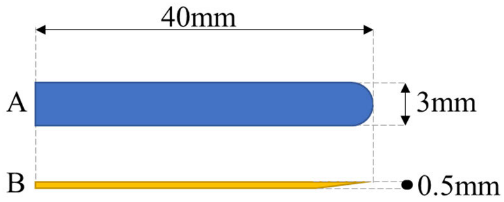

FIGURE 1. Electrodes used on the tips of the wire. A – Rounded, B – Needle. The tips are oriented vertically, pointing upwards.

The multirotor drone selected for the experiment is a DJI Phantom 4 model. This model was selected because it has enough thrust to fully deploy the wire (500g of payload) to the altitudes of interest. It offers a flight autonomy of more than 15 minutes, which is sufficient for making current measurements at different altitudes. Additionally, the drone's position control using GPS allows for pulling the wire vertically with the required accuracy.

Alongside the measurements depicted in Figure 2, potential gradient measurements are performed in some of the ground-level flights using an electrostatic field mill (EFM113B) that had been previously calibrated in the laboratory.

During the experiment, the wire is vertically unspooled as the drone goes up, maintaining a straight vertical orientation, and unwinds loosely on the floor on the way down. Therefore, only measurements during the rising flight are used for the analysis.

In terms of data logging, each sensor has its dedicated acquisition system. All sensors save data independently, which is later synchronized for analysis, as shown in the results of this paper. The RBD 9103 pico-ammeter uses the Actuel capturing software provided by the manufacturer. The DJI Phantom 4 records all its sensors' data onboard, and this data is retrieved after the flight. From these

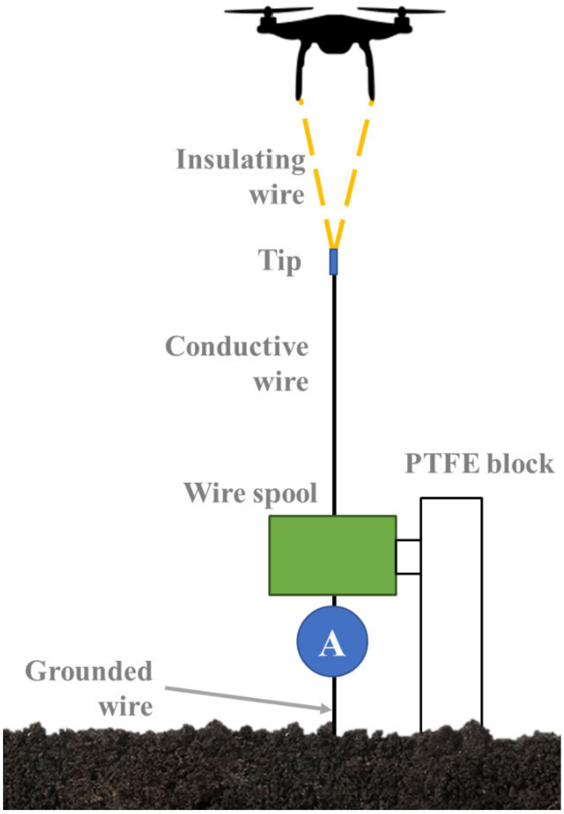

FIGURE 2. Experimental configuration diagram.

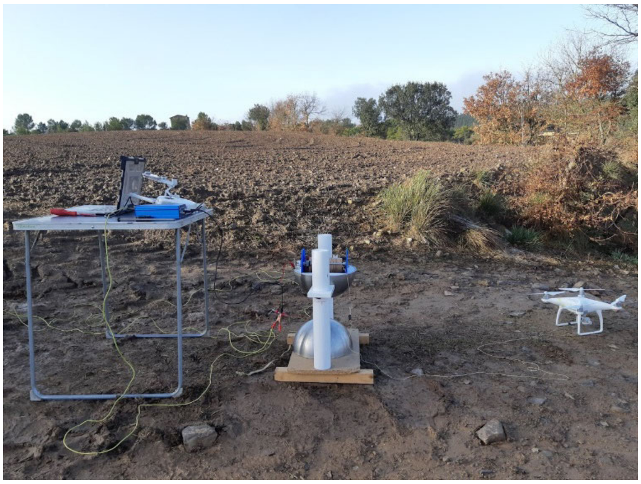

FIGURE 3. Experimental setup, with the drone on the ground ready to deploy the wire.

measurements, the drone's altitude can be used to accurately determine the wire tip altitude as a function of time and derive the vertical speed. Electrostatic field mill data is also recorded using a Picoscope 2204A oscilloscope.

In this paper, we present the results from 7 flights performed over 3 different days from a total of 30 flights conducted over 7 different days. The selection of experimental parameters and number of tests performed was selected to be able to reveal the dependencies between induced currents with altitude and vertical speed while also recreating conditions that would lead to current induction by point/corona discharge. For that reason, we performed as many flights as possible during the flight campaign, which was completed when sufficient significant data was gathered to back up the analysis. The experimental methodology followed is similar to the Placket-Burman experimental design technique described in [24], where the interdependencies of multiple factors are studied using a limited number of experiments. For example, using 12 tests, up to 11 factors could be studied if at least 2 of the factors were present in each test. In our case, all the factors (maximum of 5) are present in every test, and we performed 30 tests in total, so based on the Placket-Burman design, it should be enough data to back up our analysis. The flights that are reported in the paper, out of the 30 performed, are the ones that better summarize the observations, and the results are representative of the other flights (not shown for the sake of conciseness).

The flight experiments were conducted at a flat field in the countryside in Catalonia at 336m of elevation above sea level. The selected field was clear from interferences, including tall obstacles and sources of electromagnetic radiation like antennas that could affect the measurements. The flights were scheduled in the mornings and early afternoon when calm, or light wind conditions are more likely, to facilitate that the deployed wire stayed vertical under the drone.

The step-by-step methodology of the experiment is as follows. The first step before each flight is to initialize the sensors and data-logging devices. Next, the wire spool's physical and electrical connections are verified to ensure a proper physical connection between the wire and the drone through the Kevlar wire and an electrical connection between the wire and the pico-ammeter. After the drone takes off in each flight, the wire is vertically deployed at various vertical speeds controlled by the drone operator. During ascent, long pauses at fixed altitudes are done, with the drone hovering at a fixed position and holding the wire vertically. The hovering time at fixed positions is determined by the operator who also monitors the current induction on the wire. He makes sure that there is no change in altitude while the transient induced currents are being recorded. Finally, before the drone's battery is depleted, the drone starts to go down, and thus the experiment ends. The summary of the selected flights reported in the paper is shown below (Table 1).

III. RESULTS

In this section, we first present an overview of the measured currents in the wire during the flights. Then, we separately focus on the currents at fixed-altitude hovering flight and during ascending flight.

A. FLIGHT MEASUREMENTS

The 3rd and 4th flights are used as examples to depict the general characteristics of the measured currents. Flights 3 and 4 were performed the same day with a 2 h

TABLE 1. **Experimental flights reported in the paper. VPG stands for atmospheric vertical potential gradient.**

Day	Flight #	Tip	Time	VPG (V/m)
1	1	B – Needle	10:34am	110
	2	A – Rounded	12:24pm	130
2	3	B – Needle	07:47am	40
	4	B – Needle	09:28am	120
3	5	A – Rounded	12:26pm	20
	6	A – Rounded	12:46pm	20
	7	B – Needle	12:59pm	20

difference and the same tip. The main difference between the two flights was the atmospheric electric field. The 3rd flight started at 7:47 am, and the measured ambient vertical potential gradient (VPG) at the ground was about 40V/m, whereas, during the 4th flight, which started at 9:28 am, the measured VPG at the ground was around 120V/m. Figure 4 shows the current timelines (yellow) for flights 3 (a) and 4 (b) for a similar flight profile, the altitude of the tip above ground (blue), and the vertical speed (green).

In general, we found that whenever the drone moves vertically, there is an increase of the induced current as long as the drone maintains a non-zero vertical speed (marker a); and when the drone hovers at a fixed position (0 m/s speed), the current is observed to either remain at approximately a constant level or slowly decay (marker b).

The steady level current increases with altitude, so the higher the altitude, the higher the current (compare levels in markers c, d, and e). At the higher altitudes tested, the induced current no longer remains constant, and instead, exponential current decay is measured (marker f).

Comparing the current at the same hovering position around 100 m (marker b): the quasi-steady current for the 3rd flight was around 28 nA, whereas, during the 4th flight, the current increased to 400 nA. It can be concluded that higher currents are measured at the same altitude when the local atmospheric electric field is higher.

At altitudes below 100 m, the currents during hovering positions do not present significant decay, whereas, above 100 m, we found that the decay becomes noticeable, mainly when the atmospheric electric field is higher (flight 4). The onset of the exponential decay happens at a higher altitude for the 3rd flight (lower atmospheric fields), past 175 m. This behavior is highlighted by marker f in Figure 3. In both flights, the exponential decay has a comparable characteristic time constant of ∼160 s.

Next, flights 6 and 7 will be used to investigate the effect of the termination of the wire (electrode geometry) on the measured currents. These flights were conducted sequentially, and the ambient conditions are expected to be similar. Figure 5 shows the currents for the two flights at around the same hovering altitude (∼125-150 m). Figure 5a shows the case with the rounded tip (A), and Figure 5b displays the case with the needle tip (B). In the case of the rounded tip, the current during the hovering position dropped to zero, likely indicating the absence of point/corona discharge activity. In the subsequent flight (Figure 5b), with the needle terminating the wire, the current was of the order of 40 nA for the same hovering altitude. Moreover, this current increased with increasing hovering altitude.

Comparing these results with the flights from previous days (3rd and 4th flights), the main difference is attributed to the rounded tip, since at a hovering position of ∼150m, there is no induced current, whereas, for all other flights, a non-zero current was measured. During the 3rd day of experiments, when the 6th and 7th flights were performed, there were some clouds in the sky, and the low VPG could explain that only the sharp geometry of the tip concentrated enough charge for the onset of corona discharge at the tested hovering positions.

B. TRENDS WITH ALTITUDE AND VERTICAL SPEED

As seen in the previous section, we observed two well-differentiated sources of current induction: (i) induced currents at hovering fixed altitude positions and (ii) induced currents during vertical ascent.

Figure 6 shows the average current measured at different hovering positions for several flights. The different magnitude, across different flights, for the same altitude can be appreciated: in this case, attributed to differences in the ambient VPG. All flights show a tendency to increase the induced current with altitude up until a particular value, after which the current decreases exponentially, as shown in Figure 4 (mark f).

Figure 7 shows the induced currents against vertical speed and altitude (color and size of the data points) for the 3rd flight. Similar behavior has been observed for the other flights. Figure 7 shows that it is possible to have measured currents of the same magnitude at different altitudes, depending on the vertical speed. For instance, currents measured around 60m of altitude and 2.5m/s of vertical speed are similar to currents measured around 100m and 0.5m/s. Therefore, the induced current is both a function of altitude and vertical speed, and similar currents can be achieved for high vertical speeds at low altitudes and low vertical speeds at high altitudes.

IV. MODELLING OF ATMOSPHERIC-DRIVEN CURRENTS

A. PARTIAL DISCHARGE CURRENTS

An electrical charge is induced in a static vertical structure when exposed to the atmospheric potential in fair-weather conditions. Due to the quasi-static nature of the atmospheric potential, no currents will be associated with this effect.

Therefore, it is here hypothesized that the source for the observed currents at steady level flight can be attributed to point/corona discharge (PD). According to [25], the current, i_{PD} due to PD is given by equation (1).

$$i_{PD} = A\varepsilon_0 u V_p = A\varepsilon_0 k E_a V_p \tag{1}$$

where A is a geometry-dependent non-dimensional constant to fit, ε_0 is the air permittivity, u is the absolute ion velocity, approximated by the electric drift, kE_a, with E_a the ambient electric field and k the mobility of positive ions taken as

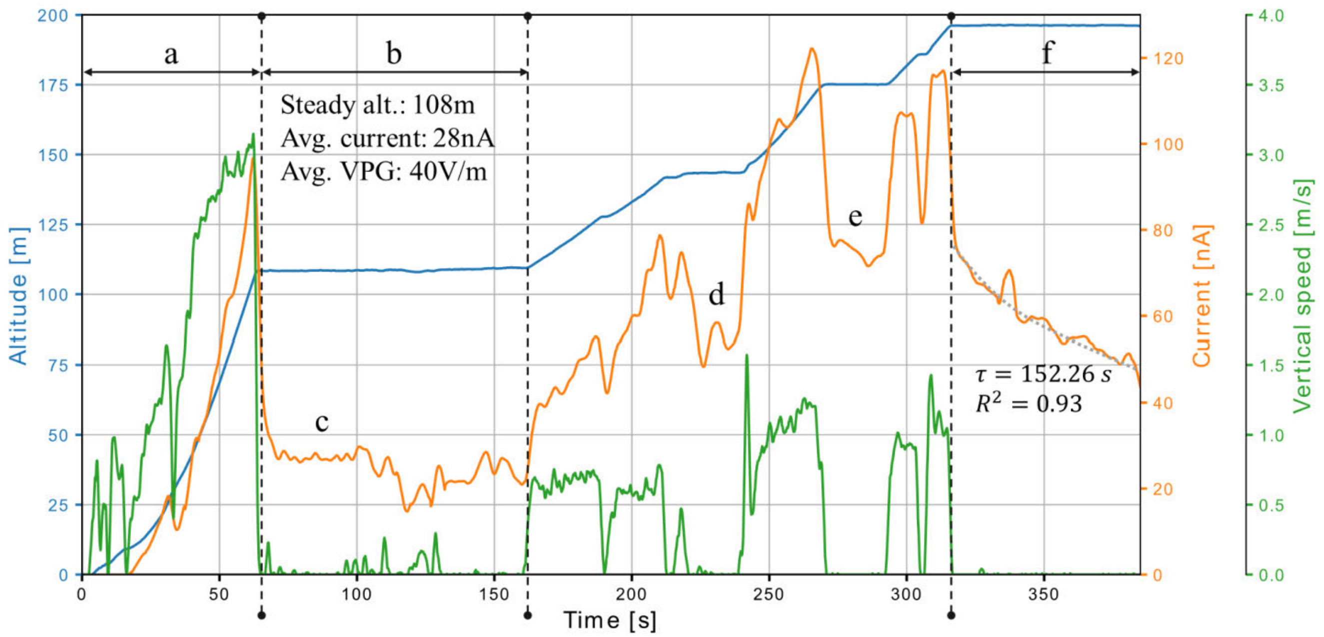

(a) 3rd flight

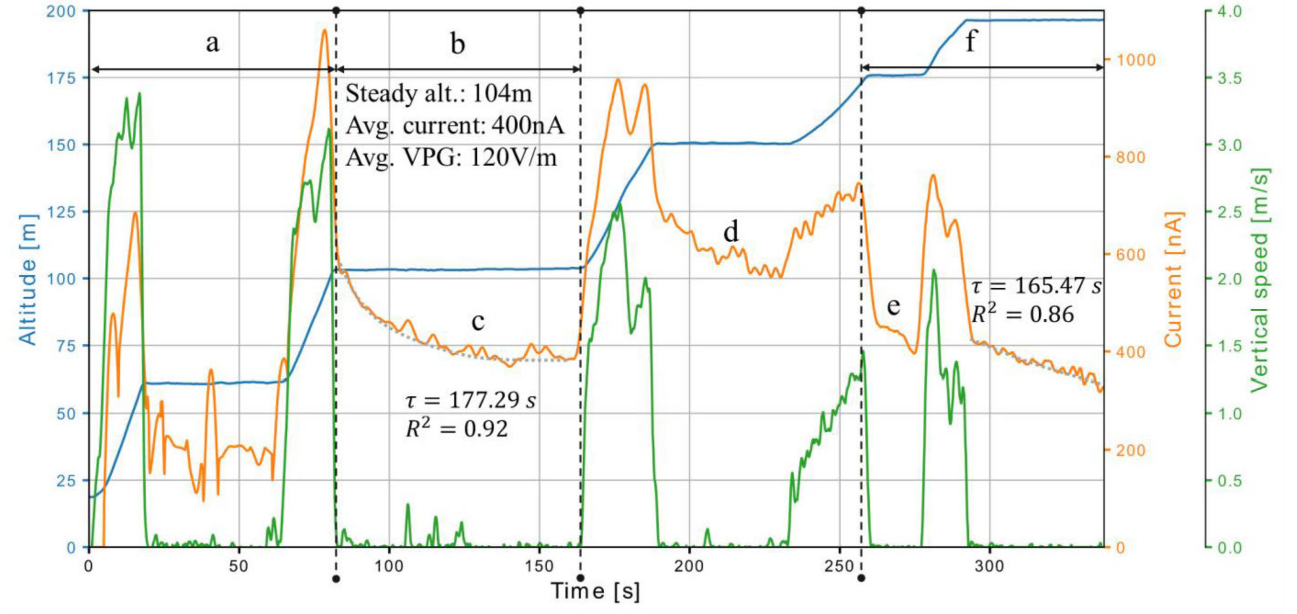

(b) 4th flight

FIGURE 4. **Current measurements alongside vertical speed and altitude of the wire tip for the 3*rd* and 4*th* flights. (*a*) Corresponds to the 3*rd* flight with VPG of 40V/m and (*b*) corresponds to the 4*th* flight with *a* VPG of 120V/m.**

$1.5 \cdot 10^{-4} m^2 s^{-1} V^{-1}$ from [25]. V_p refers to the potential at the tip of the wire expressed as, $V_p = E_a h$. The corona inception voltage is here ignored.

Applying equation (1) to the 3rd flight where the measured ambient field was $E_a = 40V/m$ and using $A = 125$ to fit the data since there is no upper limit for the coefficient in [25], results in the estimated current (*I predicted*) in Figure 8. As it can be seen, the model proposed in [25], predicts well the steady currents for the first altitude (marker a), but for higher altitudes, the rate of current increase does not match the experimental slope.

Because the wire has a sharp needle tip on top, geometry enhances the local electric field beyond the ambient value. Rather than capturing all the geometry enhancement through a constant A, we propose to use a corrected V_p where the ambient field is substituted by the enhanced electric field at

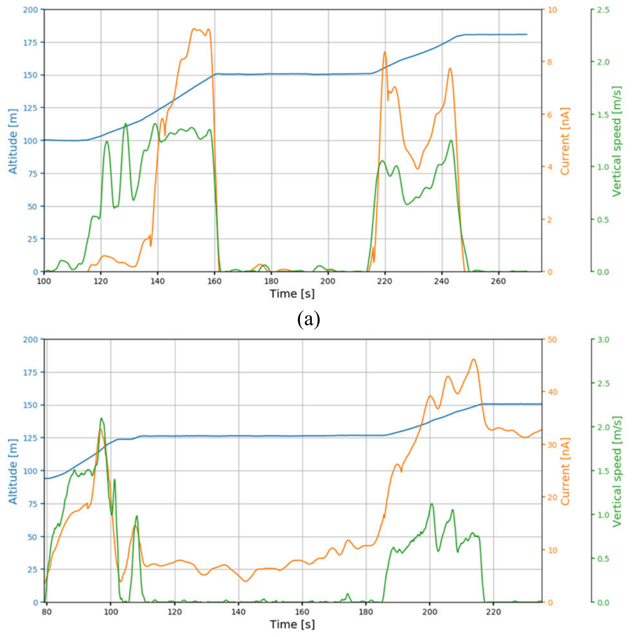

(a)

(b)

FIGURE 5. Steady height current measurements with different tips. (a) Corresponds to flight 6 with a rounded tip and (b) to flight 7 with a needle tip.

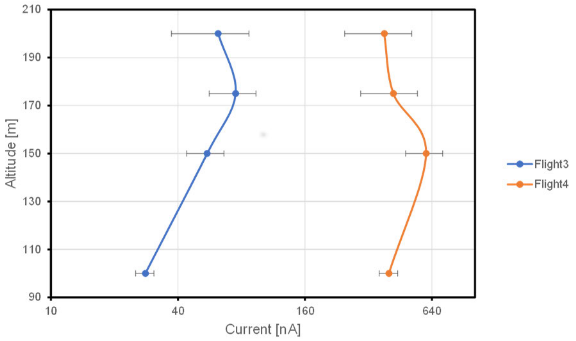

FIGURE 6. Current measurements for different flights at fixed altitude hovering positions.

the tip.

$$V_p = E_{tip} h \tag{2}$$

The enhanced electric field at the tip, E_{tip}, is obtained from an electrostatic simulation in COMSOL Multiphysics software, which is detailed in the Appendix, resulting in:

$$E_{tip} = E_0 \cdot (3.106h + 13.025) \tag{3}$$

Note that formula (3) still does not capture all of the geometry effects since the sharp tip is numerically approximated by a spherical cap of the same radius as the wire.

Furthermore, to fit equation (1) with the enhanced electric field at the tip of equation (2), the coefficient A needs to be decreased from 125 to 0.35, being out of the range proposed in [25], because most of the geometric effect is now contained in V_p. The modified predicted current (noted as I *enhanced*) appears in red in Figure 8, whereas the measured current is shown in yellow. Only the periods during which the wire is at a fixed-altitude hovering position are captured by this source of current (markers a, b, c, d on Figure 8). The PD current model accurately predicts the steady altitude currents up to 175 m for this particular flight. Above this altitude, when the current can no longer be considered constant, the model fails to predict the current (marker d). The failure in prediction is likely due to the neglection of the space charge created by the PD that reduces the local electric field. The formulation given by equation (1) assumes the absence of space charge. It is hypothesized that as the local electric field becomes stronger and the corona current increases, space charge effects can no longer be neglected, and at some point, the formulation starts to fail. Corona discharge produces a space charge that would shield the tip of the wire, decreasing the local electric field. At low currents, this contribution can be neglected, but not so at higher values. The presence of a strong corona has been confirmed in recent experiments, at altitudes similar to the ones here studied, in a wire lifting experiment [16], and similar current decays have also been observed experimentally in the laboratory [26].

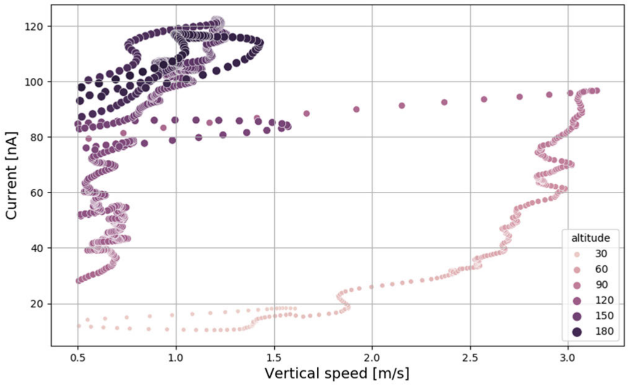

FIGURE 7. Measured current against vertical speed (v_z) and altitude (h, in meters) for flight 3.

From the analytical point of view, the space charge effects can be considered using the corona discharge model of [27]. In [27], a simplified analytical model for describing transient corona discharge is proposed and is summarized in equation (4). In this model, the ionization zone is assumed to coincide with the stressed electrode surface and is considered an unlimited source of ions. As a result, the electric field on the electrode surface is maintained at a threshold field for corona inception, E_c, which is determined from the Townsend criterion for self-sustained discharge ignition and is a function of the electrode radius. The model considers a spherical solitary stressed electrode and predicts the corona current i_A in time t.

$$i_A \approx \frac{2\sqrt{2}\pi\varepsilon_0}{3}\sqrt{\frac{k}{t}}\left(V_p - V_c\right)^{\frac{3}{2}}, \tag{4}$$

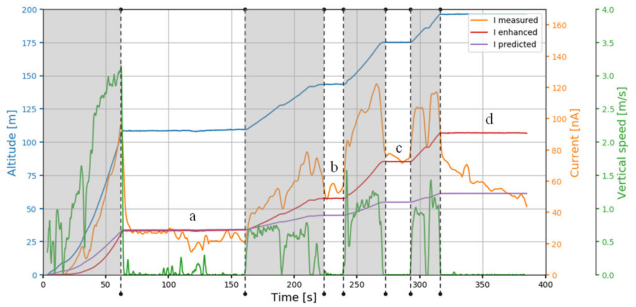

FIGURE 8. **The induced current predicted from the PD model compared to measurements during flight 3.**

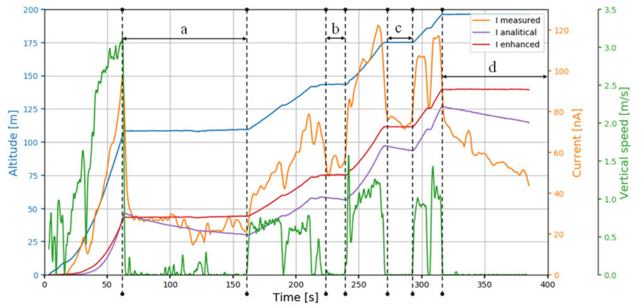

FIGURE 9. **Comparison between experimental and analytical decay formulations for flight 3.**

where $V_c = E_c h$ is the critical potential at corona discharge onset and, in general, is dependent on the geometry of the tip, and $V_p = E_{tip} h$ is taken as in equation (2). Again, k the mobility of positive ions is taken as $1.5 \cdot 10^{-4} m^2 s^{-1} V^{-1}$ from [25]. For this discussion, V_c is assumed to be much smaller than V_p (particularly as altitude is increased) and is here ignored.

Equation (4) is used to estimate the currents measured during the 3rd flight. In Figure 9, results from the predicted current by point discharge (*I enhanced*, red) and the analytical model (*I analytical*, in purple) are compared, similar to Figure 8. I enhanced predicts the base current level for hovering positions quite well (Figure 9 marks a, b, and c), but only the analytical model captures the observed decay at higher altitudes.

B. VERTICAL MOTION-INDUCED CURRENTS

This section considers the currents induced by the vertical motion of the tip. In this case, the current results from the increased induced charge as the wire penetrates the growing potential of the atmosphere. Therefore, the current will depend on the speed of the ascending wire and the potential difference between the wire and the atmosphere. Then, the velocity component of the current i_{vel} can be calculated from equation (5).

$$i_{vel} = C\left(h\right) E_a v_z \tag{5}$$

where $C(h)$ refers to the capacitance of the wire at different altitudes, detailed in the Appendix. E_a is the vertical potential gradient measured at the ground and the v_z is the vertical speed of the tip.

We will use the 5th flight to compare the measured current with the current calculated using equation (5) due to the absence of PD currents. In this case, assuming that PD does not occur during the ascending parts of the flight, the nature of the current would be only related to the change in altitude.

In Figure 10, it can be observed that the model, in general, predicts well the trends and magnitude of the current.

C. SUPERPOSITION OF CURRENT COMPONENTS

Combining models from (1) and (5), as a sum of contributing factors that induce current into the wire, the combined model is given by:

$$i = i_{PD} + i_{vel} \tag{6}$$

which applied to the 3rd flight, shows good agreement and captures the trends, Figure 11.

The superposition of the two main sources of current induction gives a very good prediction of the total induced current on the wire, but the formulation fails to capture the current decay due to the space charge accumulation nearby the tip of the wire.

To address this, and as seen in Figure 9, the analytical formulation for predicting currents at hovering positions does predict the current decay at higher altitudes. Combining (4) for hovering positions with the vertical speed induced

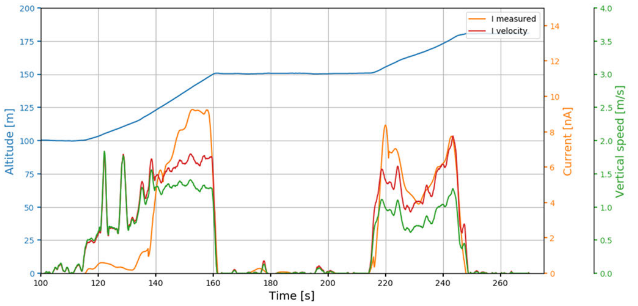

FIGURE 10. **Predicted current from the v_z model compared to measured values during flight 5.**

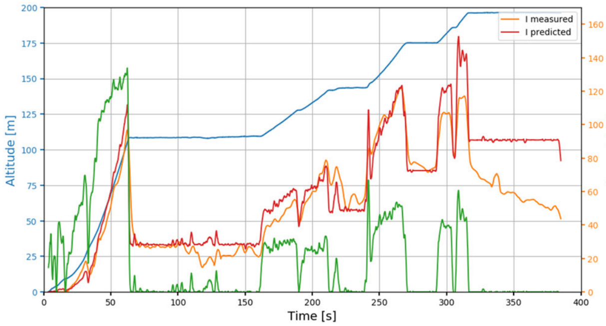

FIGURE 11. **Full model, induced current prediction with PD combined with equation (5) for vertical speed. Flight 3 case.**

currents (5) results in the equation,

$$i = i_A + i_{vel}. \tag{7}$$

Figure 12 shows predicted currents (purple) when applying (7) to the 3rd flight. Combining the analytical model and the electrostatics for the vertical speed induction predicts the induced currents on the wire very well. The decay constants predicted diverge from the measurements at high altitudes, but the magnitude of the current and overall behavior is well captured.

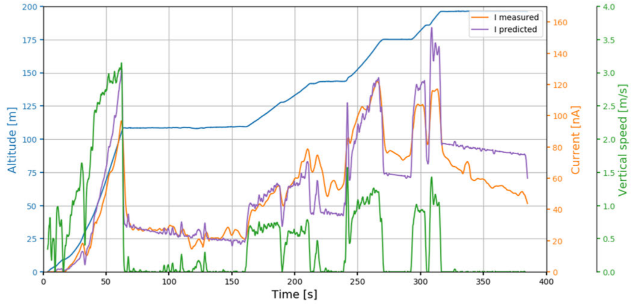

FIGURE 12. **Full model, induced current prediction combining the analytical model and equation (5) for vertical speed. Flight 3 case.**

V. DISCUSSION

A. IMPLICATIONS FOR WIND TURBINES

As stated in the introduction, wind turbines are tall structures with a large portion of their length in rotation. This translates into the blade tips constantly changing their altitude.

As it has already been observed [23], tall structures under fair-weather with relatively low potential gradients induce low currents due to point discharge phenomena, which is also dependent on the sharpness of the tip. Additionally, for wind turbines, a second source of current induction is present because of the rotation of the blades, as revealed in these experiments. Altitude variation, at a certain speed, proved to induce higher magnitude currents than point discharges and therefore is expected to dominate current induction in wind turbines compared to steady tall structures.

Indeed, measurements on a wind turbine under fair-weather conditions (personal communication) showed current levels for a static blade around 20nA (for a wind turbine of 100m height), comparable to the levels measured around 100m altitudes in the experiments done with wires.

When comparing field data for actual wind turbines to the wire experiments, the proposed flight experiment and methodology are a good proxy for simulating a wind turbine's electric response to the ambient VPG, and similar order of magnitude induced currents and trends have indeed been observed in the field. These experiments could be an inexpensive option for determining the risks to new sensors on wind turbines before they are actually installed, reducing the testing costs, i.e., complementing with experimental data numerical studies such as [28].

Additionally, measured induced currents are helpful to consider as a noise source when instrumentalizing wind turbines with sensors. From these studies, expected noise magnitudes could be estimated and introduced as an input to network-based remote wind turbines CMS, as the ones described in [3], as additional environmental information to be considered by their predicting algorithms [29]. A limitation of these experiments is that they are only valid to simulate grounded blades. Some wind turbines have electrically isolated blades, which make the blades behave as floating conductors. Recent experiments have shown that the behavior of PD from electrically-isolated electrodes can indeed be very different from the behavior of grounded systems [30]. The experimental platform will be modified in the future to consider electrically-isolated blades.

The main advantage of this experimental technique is that it provides experimental data for induced currents on wind turbines using a method that is fast and economical. It should not be viewed as a substitute for modeling software but rather as a complement that could also be used for validation studies.

From a scientific perspective, this experimental technique could also be used to gather atmospheric electricity measurements. The use of drones could improve the current methods used [31]. Deploying a conductive wire with a drone is practical for current atmospheric measurements, like the ones performed in the past with balloons and kites. However, the use of drones allows for better position and altitude control of the wire than previous techniques based on balloons and kites [9], [15]. The only disadvantage compared to other platforms is that the drone flight autonomy limits the experiment duration.

Moreover, a racing drone with higher vertical speed capabilities (around 35m/s) might be able to recreate lightning-triggering experiments, normally conducted using rockets [32], possibly with higher control over the wire deployment speed. Deployment of the wire at high speeds allows to physically simulate lighting streamers or even leaders if the discharge is fully triggered.

B. INDUCED CURRENT MODEL FOR WIND TURBINES UNDER FAIR-WEATHER

In this section, the complete current model in section section IV.C is adapted to predict currents on wind turbines using expressions (6) and (7).

Current expressions (1) and (4) will be similar for the PD current contribution, with a few caveats. The geometry-dependent constant, A in equation (1), will depend on the blade's geometry and will result in a different field enhancement. The corona inception threshold in equation (4) will also need to be revisited. For this discussion, the most notable difference is in the V_p parameter defined in (2). Whereas the wire is in a vertical motion, the blade is in rotational motion, so h, the blade tip altitude, is defined as,

$$h = l + Rcos(\theta) \tag{8}$$

where l is the nacelle altitude and R the blade's length; the definition of these parameters is also shown in Figure 13. All other parameters are here selected to be the same as for the wire experiment.

For the motion-induced current, formula (5) representing the vertical speed induced current, needs to be adapted to reflect the capacitance of the wind turbine geometry, C,

$$C = C_h(R + l) \tag{9}$$

where C_h is the capacitance per meter of the blade experimentally determined, and the experimentally determined value for the wire used in these experiments, $8.58pF/m$, will be used as a first estimation (see Appendix).

Finally, the blade tip vertical speed can be defined as,

$$v_z = \frac{\pi}{30} nRsin(\theta) \tag{10}$$

where n is the angular velocity of the wind turbine in rpm, which following Figure 13 definitions, corresponds to $\omega = \frac{\pi}{30}n$.

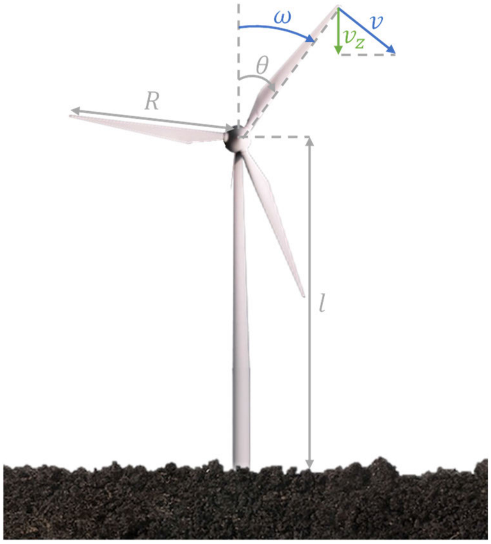

FIGURE 13. **Wind turbine geometry reference.**

The main difference when using the formulation given by (6) and (7) is that (6) does not account for the presence of space charge, but (7) does; e.g., it accounts for the shielding effect from the emitted ions, limiting the induced currents. In the case of rotating wind turbine blades, the motion of the blade ensures that it escapes the shielding effect of the emitted ions, as explained in [14]. For this reason, we propose (6) to be a better model for predicting currents of rotating wind turbines, as it ignores the presence of space charge. If the wind turbine is not in motion, (7) becomes a better model for predicting induced currents as the shielding effects of the space charge are accounted. These models are tested for possible wind turbines up to 200m high, as that was the maximum height reached with the experiments to support the model.

The results from applying (6) accounting for wind turbine-modified parameters and conditions similar to the experiments with wires are shown in Figure 14. The sample wind turbine has a length of $l = 60m$ and a blade radius of $R = 50m$, an angular velocity of $n = 10rpm$ and is exposed to an ambient VPG of 40V/m.

The total predicted current is shown in blue (I_{tot}) and the components of this current are I_{PD} (red) and I_{vel} (purple), which correspond to the currents induced because of the altitude and the vertical speed, respectively. We observed that applying (7) to the same wind turbine gives a total induced current that gradually decays, and the results were discarded due to the overemphasis on space charge effects and the fact that the blade rotation disperses the ion cloud, reducing its effect.

From Figure 14, we see that the maximum magnitude of the induced current appears at two locations: (i) a negative current when the blade tip is between its top position and the horizontal one, around angular position 60°; and (ii) a positive current when the blade tip is between its horizontal position and the vertical one, around angular position 300°. The switch in polarity of the induced current of the wind turbine is due to the orientation of the vertical speed. As already stated in this article, the current induced by the vertical motion is higher in magnitude than the current due to the PD at the blade tip. For the considered case, currents associated with the partial discharge oscillate between 30nA at the highest position of the tip and 2 nA at the lowest position; currents induced by the vertical speed oscillate between ±120nA, inverting the polarity with the vertical speed change.

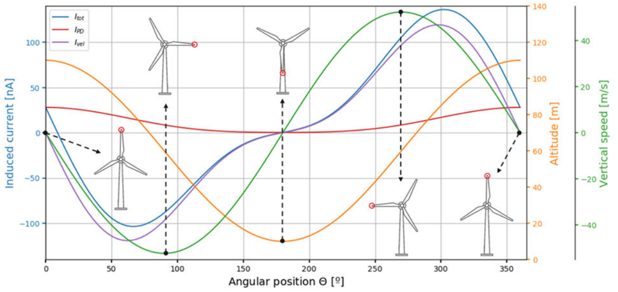

FIGURE 14. **Wind turbine induced currents predicted using the proposed model under fair-weather conditions.**

The main advantage of the models proposed in this section is that they provide simple formulas that can be easily evaluated once the main parameters of the wind turbine are defined. Currently, there is no other simple way to predict the induced currents on wind turbines due to atmospheric electricity. Using the proposed equations eliminates the need for a complex numerical model to simulate those currents. In addition, these equations could, in principle, be added to existing sensor fault detection algorithms to estimate noise levels. Also, in combination with predetermined threshold levels, these estimates could be used to determine when to disconnect sensors if they risk being damaged by ESD.

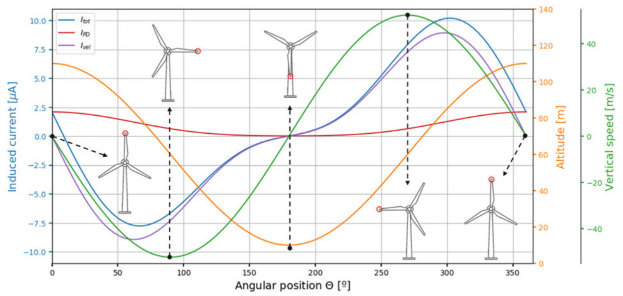

FIGURE 15. **Wind turbine-*induced* currents *extrapolated using* the proposed model under thunderstorm-weather conditions.**

C. 'EXTRAPOLATION' TO THUNDERSTORM WEATHER

The modeling work reveals that current induction has a proportional relationship with the ambient VPG. An extrapolation of the expected currents on wind turbines under thunderstorm conditions is made here, accounting for the different sources of current identified. The main parameter to be modified is the ambient VPG to a value representative of thunderstorm environments. The following exercise uses the same wind turbine as in Figure 14 but changes the VPG from 40V/m to 3kV/m, which is a typical value for thunderstorm weather. The rest of the parameters remain unchanged. Results of this extrapolation are shown in Figure 15. The expected currents are in the order of tens of microamps, increasing by two orders of magnitude compared to the fair-weather predictions. Because of their higher value, now these currents could be dangerous to people, and additionally, they are high enough to permanently damage any electronic device in contact with them [7], [33], like the new sensors installed in wind turbines for the CMS.

VI. CONCLUSION

This paper explored the applicability of a new technique deploying vertical conductors with drones to measure atmospheric electricity effects, mainly to simulate the current induction in wind turbines. A model that combines partial discharge and vertical motion contributions to the current induction process has been proposed and validated using the measured currents for the wire experiments. The model has been adapted to be used in wind turbines and showed good agreement with prior field measurements of real wind turbine currents under fair-weather performed by our team. The experimental technique proposed in this paper could be used as a low-cost testing system to evaluate the risks to new sensors to be installed on wind turbines.

Specific conclusions derived from the results are:

- Wind turbines induce much higher currents than tall structures because of their blades' rotation.
- Point discharge currents can appear under fair-weather conditions with low potential gradients at tall structures, but vertical speed induces higher magnitude currents.
- At certain threshold altitudes, and due to higher electric fields at the tip and higher discharge currents, the space charge injected by point discharge can no longer be neglected, and the current tends to decay as the space charge accumulates around the corona source. This is observed for non-moving wires/ blades.
- The experimental setup is a valuable and reliable platform for atmospheric current measurements.
- Experiments performed may be used as a test platform for simulating the conditions encountered by new sensors installed on wind turbines.
- Induced currents on wind turbines under thunderstorm conditions could be fatal to small self-powered sensors.
- Sharp geometries start inducing currents at lower ambient VPG than blunt ones.

Future work for this research will center on:

- Extension of the experiments to include electrically-isolated blades.
- Extension of the experiments to include non-conductive blade materials, including GFRP.

APPENDIX

ENHANCED ELECTRIC FIELD AT THE TIP

To calculate the enhanced electric field at the tip of the wire, an axisymmetric simulation has been performed using a Finite Element Method solver (COMSOL). A wire of the same diameter as the one that flew has been studied at multiple altitudes ranging from 0m to 150m, exposed to a VPG of 40V/m. The computational domain had a height of 200m and a width of 100m. Results from a sample simulation at 150m altitude are shown in Figure 16.

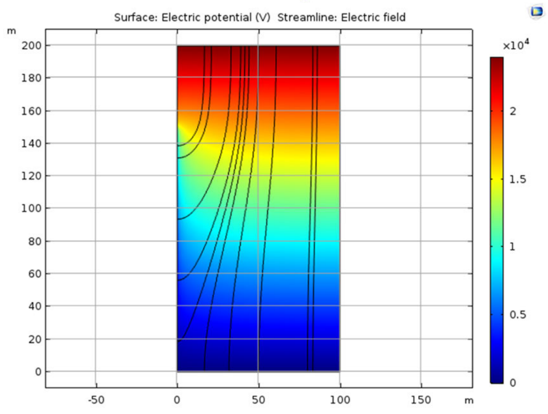

FIGURE 16. **Finite element simulation result for the local electric field enhancement at the tip of the wire.**

To quantify the enhancement of the local electric field at the tip of the wire, different altitudes have been plotted in Figure 17.

A regression line fitting of the enhanced vertical potential gradient at the tip gives expression (3), which is linear and has fitting goodness with the data points of $R^2 = 0.952$. Note that this model does not account for the total enhancement at the tip since the radius of curvature at that location is much smaller than the wire radius (not a spherical cap).

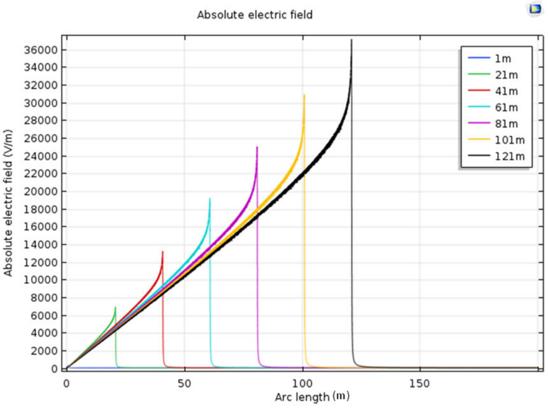

FIGURE 17. Finite element method simulation result for the electric field enhancement at the tip.

ELECTROSTATIC MODEL FOR VERTICAL SPEED MODELLING

The whole system is studied electrostatically to model the induced current on the wire because of the change in altitude. Starting from the current i definition as the variation of charge q in time t, and the capacitance definition as the variation of charge with potential ϕ, (11) is proposed as a model for the induced currents during the change in altitude of the wire.

$$\begin{cases} C = \dfrac{dq}{d\phi} \\ i = \dfrac{dq}{dt} \end{cases} \rightarrow i = C\frac{d\phi}{dt} \tag{11}$$

Then $d\phi/dt$ can be defined as,

$$\frac{d\phi}{dt} = E_a\frac{dh}{dt} = E_a v_z, \tag{12}$$

where E_a is the VPG at the ground, h the altitude and v_z the vertical speed. Combining (11) and (12), at any given altitude,

$$i = CE_a v_z. \tag{13}$$

Generalizing the formula (13), for any altitude,

$$i(h) = C(h)E_a v_z \tag{14}$$

where now the induced current on the wire will also depend on the altitude since the capacitance of the wire changes as more wire is deployed during ascent, as explained in the following section.

WIRE CAPACITANCE CALCULATION

As the wire ascends through the atmosphere, more length of it is deployed. The increase in length consequently increases its capacitance since more charges can be stored along the conductor under the influence of the atmospheric electric field. This capacitance of the wire is the same as defined by [15].

Rearranging (14) to isolate $C\,(h)$ gives,

$$C(h) = \frac{i\,(h)}{E_a v_z} \tag{15}$$

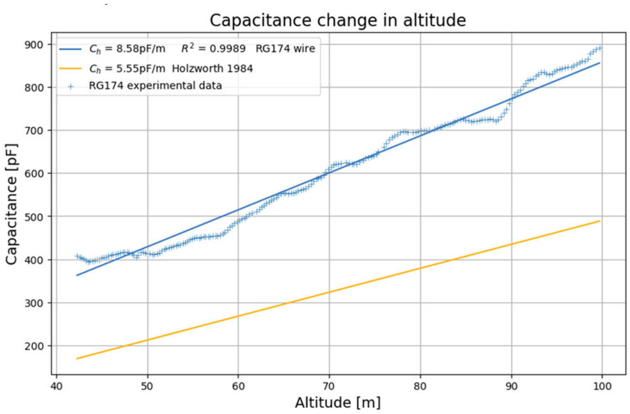

FIGURE 18. Wire capacitance changes with altitude.

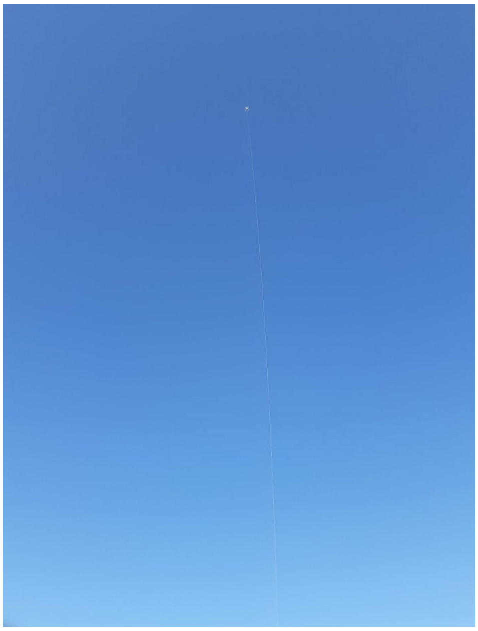

FIGURE 19. Vertical wire deployed with the drone.

then using expression (15), we can calculate the wire capacitance from the experimental data. To make this estimate, hovering positions with zero vertical speed need to be discarded. For that reason, to experimentally determine the capacitance of our system, the 4th flight has been used, exclusively using data for which the vertical speed was above 1m/s and the altitude below 100m. We know that the 4th flight has motion and altitude-induced current, but since the motion-induced current is much higher than the hovering position PD current, this flight is still valuable for approximating the wire capacitance.

The results are plotted in Figure 18, and the estimated capacitance is compared to the values reported in reference [15]. The obtained model for the 4th flight gives us higher values than the capacitance that was calculated in [15], but they are of the same order of magnitude, and the slopes are similar, indicating that differences may be attributed to different systems characteristics.

In Figure 18, the symbol C_h in the legend corresponds to the capacitance per unit length and this value times the total length gives the wire capacitance $C(h)$. The term R^2, refers to the agreement between the data and the linear regression fit. In this case, 0.9989 indicates a really good fit.

ADDITIONAL EXPERIMENT IMAGES

Detail of the deployed vertical wire with the drone.

REFERENCES

[1] P. Tchakoua, R. Wamkeue, M. Ouhrouche, F. Slaoui-Hasnaoui, T. Tameghe, and G. Ekemb, "Wind turbine condition monitoring: State-of-the-art review, new trends, and future challenges," *Energies*, vol. 7, no. 4, pp. 2595–2630, Apr. 2014.

[2] L. Lu, Y. He, T. Wang, T. Shi, and B. Li, "Self-powered wireless sensor for fault diagnosis of wind turbine planetary gearbox," *IEEE Access*, vol. 7, pp. 87382–87395, 2019.

[3] Y. Peng, W. Qiao, L. Qu, and J. Wang, "Sensor fault detection and isolation for a wireless sensor network-based remote wind turbine condition monitoring system," *IEEE Trans. Ind. Appl.*, vol. 54, no. 2, pp. 1072–1079, Nov. 2017.

[4] A. Gomez Gonzalez, P. B. Enevoldsen, A. Barlas, and H. A. Madsen, "Field test of an active flap system on a full-scale wind turbine," *Wind Energy Sci.*, vol. 6, no. 1, pp. 33–43, Jan. 2021.

[5] F. Samara and D. A. Johnson, "In-blade load sensing on 3D printed wind turbine blades using trailing edge flaps," *J. Phys., Conf. Ser.*, vol. 1037, Jun. 2018, Art. no. 052023.

[6] *ESD and the NRG Class 1 Anemometer*. Accessed: Oct. 28, 2021. [Online]. Available: https://www.nrgsystems.com/blog/esd-and-the-nrg-class-1-anemometer/

[7] J. White, D. Adams, M. Rumsey, and J. Paquette, "Deflection with inertial measurements," *Wind Energy*, pp. 1–14, Jan. 2009.

[8] D. Berg, J. Berg, J. White, B. Resor, and M. Rumsey, "Design, fabrication, assembly and initial testing of a SMART rotor," in *Proc. 49th AIAA Aerosp. Sci. Meeting including New Horizons Forum Aerosp. Expo.*, Jan. 2011, pp. 4–7.

[9] J. A. Lopez, J. Montanya, O. van der Velde, F. Fabro, and D. Romero, "Fair weather induced charges and currents on tall wind turbines and experiments with kites," in *Proc. 33rd Int. Conf. Lightning Protection (ICLP)*, Sep. 2016, pp. 1–4.

[10] A. G. Kavaz and B. Barutcu, "Fault detection of wind turbine sensors using artificial neural networks," *J. Sensors*, vol. 2018, pp. 1–11, Dec. 2018.

[11] Z. Gao and X. Liu, "An overview on fault diagnosis, prognosis and resilient control for wind turbine systems," *Processes*, vol. 9, no. 2, pp. 1–19, 2021.

[12] R. D. Gowdar and M. C. Mallikarjune Gowda, "Reasons for wind turbine generator failures: A multi-criteria approach for sustainable power production," *Renewables: Wind, Water, Sol.*, vol. 3, no. 1, pp. 1–8, Dec. 2016.

[13] F. Rachidi, M. Rubinstein, J. Montanya, J.-L. Bermudez, R. Rodriguez Sola, G. Sola, and N. Korovkin, "A review of current issues in lightning protection of new-generation wind-turbine blades," *IEEE Trans. Ind. Electron.*, vol. 55, no. 6, pp. 2489–2496, Jun. 2008.

[14] J. Montanyà, O. van der Velde, and E. R. Williams, "Lightning discharges produced by wind turbines," *J. Geophys. Res., Atmos.*, vol. 119, no. 3, pp. 1455–1462, Feb. 2014.

[15] R. H. Holzworth, "Hy-wire measurements of atmospheric potential," *J. Geophys. Res.*, vol. 89, no. 3, pp. 1395–1401, 1984.

[16] D. Hong, H. Rabat, M. J. Kirkpatrick, E. Odic, N. Merbahi, J. Giacomoni, and O. Eichwald, "Evidence of a corona discharge induced by natural high voltage due to vertical potential gradient," *Plasma Res. Exp.*, vol. 1, no. 1, Feb. 2019, Art. no. 015013.

[17] R. Davis and G. Standring, "Discharge currents associated with kite balloons," *Proc. Roy. Soc. London. Ser. A, Math. Phys. Sci.*, vol. 191, pp. 304–322, Nov. 1947.

[18] J. A. R. Fernández and J. M. Puig, "Simulation of current distribution in a wind turbine blade using the FDTD method," *Electr. Power Syst. Res.*, vol. 185, Aug. 2020, Art. no. 106350.

[19] *Wind Turbine Generator Systems—Part 24: Lightning Protection*, document IEC TR 61400-24, 2020.

[20] J. Montanya, J. A. Lopez, P. Fontanes, M. Urbani, O. Van Der Velde, and D. Romero, "Using tethered drones to investigate ESD in wind turbine blades during fair and thunderstorm weather," in *Proc. 34th Int. Conf. Light. Prot. (ICLP)*, Sep. 2018, pp. 1–4.

[21] P. Fontanes, J. Montanya, M. Arcanjo, and M. Urbani, "Experiments lifting vertical wires with drones to study wind turbines current induction and charging," in *Proc. 35th Int. Conf. Lightning Protection (ICLP) 16th Int. Symp. Lightning Protection (SIPDA)*, Sep. 2021, pp. 1–6.

[22] B. Glushakow, "Turbine generators," *IEEE Trans. Energy Convers.*, vol. 22, no. 1, pp. 214–222, Feb. 2007.

[23] M. Arcanjo, J. Montanyà, M. Urbani, V. Lorenzo, and N. Pineda, "Observations of corona point discharges from grounded rods under thunderstorms," *Atmos. Res.*, vol. 247, Jan. 2021, Art. no. 105238.

[24] R. L. Plackett and J. P. Burman, "The design of optimum multifactorial experiments," *Biometrika*, vol. 33, no. 4, pp. 305–325, 1946.

[25] S. Chapman, "The magnitude of corona point discharge current," *J. Atmos. Sci.*, vol. 34, no. 11, pp. 1801–1809, Nov. 1977.

[26] D. Wang, L. Du, and C. Yao, "Statistical study on space charge effects and stage characteristics of needle-plate corona discharge under DC voltage," *Energies*, vol. 12, no. 14, 2019.

[27] N. L. Aleksandrov, E. M. Bazelyan, M. M. Drabkin, R. B. Carpenter, and Y. P. Raizer, "Corona discharge at the tip of a tall object in the electric field of a thundercloud," *Plasma Phys. Rep.*, vol. 28, no. 11, pp. 953–964, Nov. 2002.

[28] R. D. Goud, T. Auditore, R. Rayudu, and C. P. Moore, "Frequency domain analysis of a wind turbine generator earthing system for lightning discharge currents," *IEEE Access*, vol. 7, pp. 60501–60512, 2019.

[29] K. Xiahou, Y. Liu, L. Wang, M. S. Li, and Q. H. Wu, "Switching fault-tolerant control for DFIG-based wind turbines with rotor and stator current sensor faults," *IEEE Access*, vol. 7, pp. 103390–103403, 2019.

[30] C. Guerra-Garcia, N. C. Nguyen, T. Mouratidis, and M. Martinez-Sanchez, "Corona discharge in wind for electrically isolated electrodes," *J. Geophys. Res., Atmos.*, vol. 125, no. 16, pp. 1–14, Aug. 2020.

[31] K. A. Nicoll, "Measurements of atmospheric electricity aloft," *Surv. Geophys.*, vol. 33, no. 5, pp. 991–1057, Sep. 2012.

[32] X. Qie and R. Jiang, "Triggering lightning experiments: An effective approach to the research of lightning physics," *J. Aerosp. Lab.*, vol. 5, pp. 1–12, Dec. 2012.

[33] Y. M. Hernández, T. E. Tsovilis, F. Asimakopoulou, Z. Politis, W. Barton, and M. M. Lozano, "A simulation approach on rotor blade electrostatic charging and its effect on the lightning overvoltages in wind parks," *Electr. Power Syst. Res.*, vol. 139, pp. 22–31, Oct. 2016.

POL FONTANES received the B.S. and S.M. degrees in aerospace engineering from the Universitat Politècnica de Catalunya (UPC), in 2017 and 2019, respectively, where he is currently pursuing the Ph.D. degree (industrial). He is working as a Researcher at Labelec and UPC. He is studying how electrostatic charge influences lightning attachment to aircraft and wind turbines.

JOAN MONTANYÀ received the B.S. degree in industrial engineering and the M.S. and Ph.D. degrees in electrical engineering from the Polytechnic University of Catalonia, Barcelona, Spain, in 2000 and 2004, respectively. He joined the Department of Electrical Engineering, Polytechnic University of Catalonia, as an Adjunct Lecturer, in 1997, where he is currently a Full Professor. He did several short stays at The University of Arizona, Tucson, AZ, USA; the Laboratoire d'Aerologie, Toulouse, France; and the Massachusetts Institute of Technology, Cambridge, MA, USA. He is the Head of the UPC Lightning Research Group. He is the author and the coauthor of more than 170 conferences and 52 journal publications related to atmospheric electricity including, lightning protection, lighting physics, thunderstorm electrification, severe weather, lightning warning, transient luminous events, terrestrial gamma-ray flashes (TGF), high-energy radiation from lightning and laboratory sparks, and Schumann resonance. He has participated in more than 16 research projects being the Principal Investigator of 12 projects. Seven of these projects are related to the Atmosphere-Space Interactions Monitor (ASIM), an ESA Mission. Since 2014, he has been a member of the International Conference on Lightning Protection (ICLP) and the International Commission on Atmospheric Electricity (ICAE). He is also a member of several international standardization groups for lightning protection. He was a Convener of the EU CENELEC TC81X/WG5 for the standard EN 50536' protection against lightning and thunderstorm warning systems. He is an Active Member of the IEC TC 88 PT 24 about lightning protection of wind turbines. He is also active in several CIGRE SC C4 committees, including the committee WG C4.409 related to lightning protection of wind turbine blades, the WG C4.410 about lightning to very tall objects, and the WG C4.36 related to winter lightning.

MARCELO ARCANJO received the B.S. and M.S. degrees in electrical engineering from the Federal University of Minas Gerais (UFMG), in 2016 and 2018, respectively. He is currently pursuing the Ph.D. degree with the Polytechnic University of Catalonia (UPC), in partnership with the lightning protection services company INGESCO Ltd., as part of the Marie Sklodowska-Curie Action Project titled "Science and Innovation with Thunderstorms (SAINT)." The main goal of his project is to develop novel sensors that integrate protection with information about lightning. He has been investigating features of corona discharges, leader discharges, and lightning strikes at grounded rods, mainly focused on the electric current signature of these phenomena.

MICHELE URBANI received the B.S. and M.S. degrees in physics from the University of Padua, in 2013 and 2016, respectively, with an experimental curriculum in nuclear and astroparticle physics, and the Ph.D. degree in electrical engineering from the Polytechnic University of Catalonia (UPC), in 2021. He is currently involved in the Marie Sklodowska-Curie Action (MSCA-ITN) European Project "Science and INnovation with Thunderstorms (SAINT)" as an Early-Stage Researcher at UPC. The main goal of his Ph.D. project is to study the high-energy radiation from natural lightning. He has designed and developed a VHF Broadband interferometer to map with high resolution the lightning propagation and measure in coincidence the high-energy emissions with NaI(Tl) detectors. His research interests include electrodynamics, lightning physics, and computational physics.

CRISTIAN ASENSIO received the B.S. degree in aerospace engineering from the Universitat Politècnica de Catalunya (UPC), in 2021. He is currently studying corona discharge on static wicks.

CARMEN GUERRA-GARCIA received the degree in aeronautical engineering from the Polytechnic University of Madrid, in 2007, and the S.M. and Ph.D. degrees in aeronautics and astronautics from the Massachusetts Institute of Technology (MIT), in 2011 and 2015, respectively.

She is currently the Atlantic Richfield Career Development Professor in energy studies at the Massachusetts Institute of Technology (MIT). She is an Assistant Professor with the Department of Aeronautics and Astronautics, MIT, and leads the Aerospace Plasma Group. Prior to this appointment, she worked as a Research Engineer at Boeing Research and Technology Europe, held a postdoctoral appointment at MIT, and was a Visiting Researcher at Princeton University. Her research interests include intersection of aerospace engineering, low-temperature plasma technologies, and gas discharge physics. Her current efforts span from aircraft safety issues (interaction of lightning with aircraft) to plasma technologies for ignition and combustion and combine multi-physics modeling, computation, and experimentation. She is a Senior Member of the American Institute of Aeronautics and Astronautics. She has been a recipient of several awards, including the Office of Naval Research Young Investigator Award (2021), the International Fulbright Science and Technology Award (2009–2012), and the Amelia Earhart Award (2012).

• • •